Single-Cell-Based Models in Biology and Medicine
ed. by A.R.A. Anderson, M.A.J. Chaplain, K.A. Rejniak
*Mathematics and Biosciences in Interaction*, 79–106


# II.1 Magnetization to Morphogenesis: A Brief History of the Glazier–Graner–Hogeweg Model

James A. Glazier, Ariel Balter and Nikodem J. Popławski

**Abstract.** This chapter discusses the history and development of what we propose to rename the Glazier–Graner–Hogeweg model (*GGH model*), starting with its ancestors, simple models of magnetism, and concluding with its current state as a powerful, cell-oriented method for simulating biological development and tissue physiology. We will discuss some of the choices and accidents of this development and some of the positive and negative consequences of the model's pedigree.

## 1. Introduction

Living cells, despite their great internal molecular complexity, do a few basic things. They stick to each other, move actively up and down gradients in their external environment, change shape and surface properties, exert forces on each other and their environment, secrete and absorb materials, differentiate, grow, divide, and die. A few may send electrical signals or perform other specialized functions. Many approaches to building physical models of tissues are possible. The GGH model uses a framework derived from statistical mechanics to describe cell behaviors, a choice which is not at all obvious at first glance.

The GGH model is a *cell-oriented*, as opposed to a *continuum* or *pointillistic* model. Continuum models ignore cells and treat tissues as continuous materials with specific mechanical properties, completely ignoring the division of tissues into cells. Pointillistic models treat biological tissues as collections of point-like cells, ignoring many cell characteristics that are important to biological behaviors, such as cell geometry and the adhesive interactions between cells at their membranes. While both approaches are convenient and have had many successes in explaining tissue development and physiology [33, and references therein], many biological structures have length scales of a few cell diameters, *e.g.*, capillaries or pancreatic islets, and thus require explicit spatial descriptions of cells.

The GGH model is actually a framework for defining biological models rather than a single model. GGH models define a biological structure consisting of the configuration of a set of *generalized cells*, each represented on a *cell lattice* as a

domain of lattice sites sharing the same *cell index* (generalized cells may represent all or part of a real cell or any non-cellular material in the simulation), a set of *internal cell states* for each cell (which may be quite complex), and a set of *auxiliary fields* (which may include diffusing chemicals, extracellular matrix (*ECM*), gravity, *etc.*). The heart of the GGH model is an *effective energy* or *Hamiltonian*, which encapsulates almost all interactions between model elements, and optionally, a set of partial differential equations (*PDE*s) and boundary conditions to describe the evolution of the fields, and a description of the evolution of the internal cell states. Terms in the effective energy often take the form of potential energies and elastic constraints. We call the energy *effective* because its terms primarily describe cell responses, which may not result from external forces (*e.g.*, when a cell uses its internal motile apparatus to move up or down a gradient of a chemical diffusing in extracellular space (*chemotaxis*), or attached to a substrate (*haptotaxis*)).[1] The GGH model also uses a few extra mechanisms, the most important of which is cell division. The generalized-cell configuration evolves through stochastic changes at individual lattice sites to minimize the effective energy. The classical GGH model uses a *modified Metropolis algorithm* for this evolution. Since the GGH model uses the cell as its natural level of abstraction and treats subcellular behaviors phenomenologically, it reduces the interactions among the $10^5$–$10^6$ gene products within each cell to a set of governing equations for the variation of the roughly ten phenomenological behaviors we mentioned above. A key benefit of the GGH formalism is that we can include almost any biological mechanism or cell behavior we like, simply by adding appropriate terms to the effective energy. The GGH model then automatically handles the interactions between mechanisms (though we must be aware that its choices may not be the ones that we expect or want). Thus, the GGH model provides a compact and efficient way to describe complex biological phenomena. [2]

The global parameters of the effective energy and those describing the properties of cells may be static, or evolve according to simple or complex descriptions of biological or non-biological processes. *E.g.*, the adhesion of cells might depend on a model of cell signalling written in the form of reaction-kinetics (*RK*) coupled ordinary differential equation (*ODE*s), or the growth of cells might depend on a neural-network model of genetic regulatory pathways. The GGH model itself is agnostic about the models run inside each cell or outside the cell lattice, using its Hamiltonian to translate the information those models provide into physical structure and physiological behaviors [18, 19].

Glazier and François Graner derived their model as an extension of the *large-q Potts model* of statistical mechanics [17, 16], calling it the *Extended Potts model* and later the *Cellular Potts model* (*CPM*). The name Potts associates the CPM

[1] Cells can also haptotax in response to gradients in substrate texture or rigidity.

[2] The elements of the GGH model are separable. *E.g.*, we could use a GGH Hamiltonian and evolve it in a *lattice-free* way using a Finite-Element (*FE*) method (see chapter II.4, section 1.5), or we could use a force-based formalism instead of a Hamiltonian formalism and evolve it on-lattice using the modified Metropolis algorithm.

with statistical models of equilibrium domain formation, which was appropriate to Glazier and Graner's simple version. Later extensions to the model to describe cell behaviors mean that it now has little in common with its Potts ancestor. Key differences between the Potts and GGH models include:

1. A shift from calculating static equilibrium statistics to kinetics. While the modified Metropolis dynamics (which the GGH model uses to evolve a single configuration quasi-deterministically) derives from the Metropolis algorithm traditionally used with the Potts model, it does not obey the detailed-balance conditions required to generate equilibrium ensembles.
2. Initial conditions emulating a particular biological configuration rather than random initial conditions.
3. A shift from physically-motivated to biologically-motivated domain properties. *E.g.*, biological cells remain connected, while Potts cells do not, so GGH models often include mechanisms to enforce domain connectivity.

Because the GGH model's behaviors and goals are almost totally different from those of the Potts model, the analogy which the Potts name suggests is misleading. Therefore, we propose to name it after its originators, Glazier and Graner and the person who has done the most to extend it and bring it to its current prominence in biological modeling, Paulien Hogeweg. From its ancestors, the GGH model has inherited a number of peculiarities; we will discuss several of these and possible solutions to some in sections 6 and 7. Because of its flexibility, extensibility and ease of use, the GGH model has become the single most widely used cell-level model of tissue development [18, 19, 20, 21, 31, 32, 50].

## 2. Historical Origins of the Glazier–Graner–Hogeweg Model

The GGH model began as an extension of the large-q Potts Model, itself an extension of the *Ising Model*, a simple early model of ferromagnetism based on the magnetic moments, or *spins* ($\sigma$), of individual atoms and their interaction energies ($J$). The interaction between a single pair of neighboring spins is often called a *link*, or a *bond*. Spins interact via an energy function called a *Hamiltonian*, $\mathcal{H}$. Historical usage explains many of the otherwise obscure choices of terms and symbols in the mathematical formalism of the GGH model. We begin our historical survey with the progenitor of the GGH model, the Ising model of magnetism.

### 2.1. Ferromagnetism and the Ising Model

**2.1.1. Ferromagnetism.** Ferromagnetic materials develop a permanent magnetic field from a net orientation of the quantum-mechanical spins ($\sigma$) of their component atoms. The main goal of early statistical-mechanical models of magnetism was to explain the *2nd-order* (continuous) phase transition which occurs in iron at the *Curie temperature* ($T_c$). Below this temperature, materials such as iron are *ferromagnetic*. In ferromagnetic materials, stable *domains* (connected, spatially-extended areas with coaligned spins) form without an external field, giving a net

magnetic polarization. For temperatures above $T_c$, thermal energy disrupts domain formation, the material becomes paramagnetic and its spontaneous magnetization drops suddenly to zero.

**2.1.2. The Ising model.** Ernst Ising constructed a simple model of magnetization by making four radical simplifications [24]:

1. His atoms reside at regularly spaced points $\vec{i}$ on a lattice (throughout this chapter, the symbols $\vec{i}$, $\vec{j}$, $\vec{k}$ will denote two- or three-dimensional (*2D* or *3D*) vectors of positive integers indexing lattice sites, *e.g.*, $\vec{i}$=$(k,l,m)$: $k,l,m \in \mathbb{N}$).
2. Spins have only two allowed orientations, *up* ($\sigma = 1$) and *down* ($\sigma = -1$).
3. Each atom only interacts with its nearest neighbors on the lattice.
4. The interactions are classical, rather than quantum-mechanical, so the spins obey Boltzmann statistics.

According to item 4 the relative probability of any configuration of spins $\{\sigma(\vec{i})\}$ is its *Boltzmann probability*, which depends on the configuration energy, or (Hamiltonian), $\mathcal{H}(\{\sigma(\vec{i})\})$:

$$P(\{\sigma(\vec{i})\}) = e^{-\frac{\mathcal{H}(\{\sigma(\vec{i})\})}{kT}}, \tag{1}$$

where $k$ is Boltzmann's constant and $T$ is the *temperature* in degrees Kelvin.[3] Thus, the higher the energy of a configuration, the less probable it is. In the absence of any external field, the Ising Hamiltonian is the sum of interactions $J(\sigma(\vec{i}),\sigma(\vec{j}))$ between all pairs of spins $(\vec{i},\vec{j})$ that are nearest-neighbors ($|\vec{i}-\vec{j}|$=1):

$$\mathcal{H}_{\text{Ising}} = \frac{1}{2} \sum_{(\vec{i},\vec{j})\ \text{neighbors}} J(\sigma(\vec{i})\sigma(\vec{j})). \tag{2}$$

The factor of $\frac{1}{2}$ comes because the summation double counts the interactions. In the Ising model $J(\sigma(\vec{i}),\sigma(\vec{j}))$ favors co-aligned neighbor spins (energy $-J$) and penalizes anti-aligned neighbors (energy $+J$), so we can write Eq.(2) as:

$$\mathcal{H}_{\text{Ising}} = -\frac{J}{2} \sum_{(\vec{i},\vec{j})\ \text{neighbors}} \sigma(\vec{i})\sigma(\vec{j}). \tag{3}$$

Lars Onsager analytically solved the Ising model in 2D and showed that the expected ferromagnetic phase transition did occur [38]. No analytical solution is known in 3D; however, a ferromagnetic phase transition still occurs for $T_c > 0$.

In the Ising model, the transition between ferromagnetic and paramagnetic states occurs because each unit of boundary between domains of opposite spin costs an energy $2J$, so configurations with contorted domain boundaries and many domains have higher energies than those with fewer, smoother domains. On the other hand, the number of configurations composed of many contorted domains is much larger than the number composed of a few smooth domains. If we pick a configuration at random from such an ensemble of configurations distributed

[3]From now on, we will set $k = 1$, which is equivalent to measuring temperature in units of energy, and omit $k$ from our equations.

according to the Boltzmann probability in Eq.(1), the domain structure we expect to find depends on the product of the multiplicity of the structure with the Boltzmann probability. If $T \gg 2J$, the greater number of random configurations wins out over their smaller Boltzmann factors, so random configurations are much more probable. At low temperatures, the cost of domain boundaries is so high that the lower Boltzmann probabilities of random configurations overcomes their large number, and large-domain configurations dominate. In the limit that $T \to 0$, the most probable state has all the spins in the same direction (one infinite domain).

**2.1.3. Summary.** The Ising model contains two key ideas that carry forward to the GGH model:

1. The energy of mismatched links between neighboring spins on a lattice represents the energy per unit length of the boundaries between domains.
2. A temperature or *fluctuation amplitude* determines the probability of a configuration.

However, the Ising model is far from being a model of biological cells because:

1. It lacks dynamics.
2. Many domains may share the same spin, while for biological modeling we need a unique label for each cell.

### 2.2. The Potts Model

Renfrey B. Potts, in his PhD thesis, described a simple extension of the Ising model which allowed multiple *degenerate* values of the spin, (*i.e.* the energy of a link depends only on whether the neighboring spins are the same or different and not on their particular values) [40, 41]. We can write the Potts version of Eq.(2) as:

$$\mathcal{H}_{\text{Potts}} = J \sum_{(\vec{i},\vec{j})\ \text{neighbors}} (1 - \delta(\sigma(\vec{i}), \sigma(\vec{j}))), \tag{4}$$

where $\delta(x, y) = 0 \,\text{if}\, x \neq y \,\text{and}\, 1 \,\text{if}\, x = y$. We denote the number of possible spin values by $q$. The Potts model has ferromagnetic and other phase transitions [6, 71]. In the limit of large $q$, the Potts model can have many coexisting domains at low temperatures, but multiple domains can still share the same spin and it still lacks the concept of dynamics.

**2.2.1. Summary.** The Potts model contains two key idea for biological simulations:

1. Individual domains can have individual spins (which in CPM and GGH simulations we refer to as *cell indices*.)
2. Domains have a boundary energy that can be used to model adhesivity.

However, the Potts model still has several shortcomings as a basic biological simulation:

1. It still lacks dynamics.
2. Many domains can share a single spin. In biological simulations we require that each separate domain represent a unique object, such as a biological cell or part of one.

3. The Potts model specifies only a single contact energy between all spin values.
4. The Potts model does not have a way to control domain size and shape.

### 2.3. From Statistics to Kinetics

According to statistical mechanics, the distribution of equilibrium configurations of a set of classical spins depends only on the Hamiltonian and the temperature. Mathematically, we encapsulate the statistics for all configurations in the *partition function*, which sums the Boltzmann probabilities of every configuration:

$$\mathcal{Z} = \sum_{\{\sigma(\vec{i})\}} e^{-\frac{\mathcal{H}(\{\sigma(\vec{i})\})}{T}}. \tag{5}$$

Then the *expectation value* for any function $f(\{\sigma(\vec{i})\})$ is:

$$\langle f \rangle = \frac{\sum_{\{\sigma(\vec{i})\}} f(\{\sigma(\vec{i})\}) e^{-\frac{\mathcal{H}(\{\sigma(\vec{i})\})}{T}}}{\mathcal{Z}}. \tag{6}$$

**2.3.1. Monte-Carlo methods.** Unless the partition function and the relevant expectation values are soluble analytically, which is rare, we must evaluate them numerically, which is effectively impossible because of the enormous number of configurations to enumerate (in the Potts model, $q^N$, where $N$ is the number of spins in the lattice). Computationally, Ashkin and Teller showed that we can neglect the vast majority of configurations which have high energies and thus very low probabilities, making the calculation tractable [5]. In their *Monte-Carlo* method, we start with any lattice configuration and 'jump' randomly from configuration to configuration with probabilities chosen so that the number of times we visit a configuration is proportional to its Boltzmann probability. If we then average the values of $f$ that we calculate for such a sequence of configurations, the average converges to $\langle f \rangle$. In effect, we have replaced an integral over configurations with a time average. However, because the Ashkin–Teller method allows jumps between any two configurations, it still lacks the intrinsic time order that kinetic models require. The required probability for a transition between configurations $\{\sigma(\vec{i})\}$ and $\{\sigma'(\vec{i})\}$ is:

$$\frac{p(\{\sigma(\vec{i})\} \to \{\sigma'(\vec{i})\})}{p(\{\sigma'(\vec{i})\} \to \{\sigma(\vec{i})\})} = \frac{e^{\mathcal{H}(\{\sigma(\vec{i})\})/T}}{e^{\mathcal{H}(\{\sigma'(\vec{i})\})/T}}. \tag{7}$$

This condition is called *detailed balance*. Monte-Carlo methods do not obey detailed balance at $T = 0$.

**2.3.2. The Metropolis algorithm.** The *Metropolis algorithm* [35] radically modifies the Ashkin–Teller method because it is *local*; *i.e.*, instead of allowing transitions between any two configurations, it allows transitions only between configurations differing in their spin value at a single lattice site. We can think of the Metropolis algorithm as diffusion in configuration space. This local behavior allows a natural time ordering of configurations, because any configuration retains a memory of past configurations, and limits allowed future configurations. The Metropolis algorithm for a Hamiltonian, $\mathcal{H}$ is:

1. Choose a lattice site at random. We call this the *target site*, which we wil denote $\vec{i}_{\text{target}}$ and its spin, the *target spin*, which we will denote $\sigma_{\text{target}}$.
2. Pick any value of spin at random. We call this spin the *trial spin* and denote it $\sigma_{\text{trial}}$.
3. Calculate the current configuration energy, $\mathcal{H}_{\text{initial}}$, and the energy of the configuration if the target spin were changed to the trial spin value, $\mathcal{H}_{\text{final}}$.
4. Calculate the change this substitution would cause in the total energy, *i.e.*
$$\Delta\mathcal{H} = \mathcal{H}_{\text{final}} - \mathcal{H}_{\text{initial}}, \tag{8}$$
5. Accept this change (*i.e.* really change the spin value at the lattice site) with probability:
$$p(\sigma(\vec{i}_{\text{target}}) = \sigma_{\text{target}} \to \sigma(\vec{i}_{\text{target}}) = \sigma_{\text{trial}}) = \begin{cases} 1 & \text{if } \Delta\mathcal{H} < 0, \\ e^{-\Delta\mathcal{H}/T} & \text{if } \Delta\mathcal{H} > 0. \end{cases} \tag{9}$$
Steps 1 through 5 together are called a *spin-copy attempt*.
6. Go to 1.

On a lattice with $N$ sites, we define one *Monte-Carlo step* (*MCS*) as $N$ spin-copy attempts. We also define the *acceptance rate* to be the average ratio of the number of spin copies accepted to the number of spin-copy attempts. If the acceptance rate is small (as a rule of thumb, the acceptance rate should be greater than 0.01), the Monte-Carlo method is inefficient and we say that the computation is *stiff* for that Hamiltonian. Clearly, the acceptance rate increases as $T$ increases. For $T > 0$ (because the transition probability, Eq.(9) obeys Eq.(7), the long-term distribution of configurations obeys Boltzmann statistics, Eq.(1).

**2.3.3. The use of the Metropolis algorithm for quasi-deterministic kinetics.** Two behaviors suggest the possibility of using the Metropolis algorithm for kinetic simulations:

1. While the long-time behavior of the Metropolis algorithm is purely statistical, at low temperatures, over short times, the transition probability tends to lower the configuration energy.
2. For $T = 0$, the Metropolis algorithm does not produce a statistical equilibrium. Instead it drives the configurations down energy gradients to a local energy minimum, where evolution stops.

Consider a sequence of configurations, each differing by one spin value, $\{\vec{S}_1, \vec{S}_2, ...\}$, with associated energies, $\{\mathcal{H}_1 > \mathcal{H}_2 > ...\}$. Then the net *rate of transition* (the difference between the forward and backward transition probablilities):
$$r(\vec{S}_i \to \vec{S}_{i+1}) = p(\vec{S}_i \to \vec{S}_{i+1}) - p(\vec{S}_{i+1} \to \vec{S}_i) = 1 - e^{\frac{-\mathcal{H}_i + \mathcal{H}_{i+1}}{T}}. \tag{10}$$
If we choose $T$ such that $\frac{\mathcal{H}_i - \mathcal{H}_{i+1}}{T}$ is small, but not too small, for all $i$, [4] then,
$$1 - e^{\frac{-\mathcal{H}_i + \mathcal{H}_{i+1}}{T}} \sim \frac{\mathcal{H}_i - \mathcal{H}_{i+1}}{T} + \mathcal{O}((\frac{-\mathcal{H}_i + \mathcal{H}_{i+1}}{T})^2), \tag{11}$$

[4]The existence of such a $T$ depends on energies being similar for nearby configurations, which is true for Ising, Potts, CPM and GGH Hamiltonians.

so the net rate:

$$r(\vec{S}_i \rightarrow \vec{S}_{i+1}) \sim \mathcal{H}_i - \mathcal{H}_{i+1}. \tag{12}$$

In this case, if we take one spin-copy attempt as our time unit, the average *speed* from $\vec{S}_i \rightarrow \vec{S}_{i+1}$ is:

$$vel(\vec{S}_i \rightarrow \vec{S}_{i+1}) = \frac{1}{T}\vec{\nabla}\mathcal{H} \cdot (\vec{S}_{i+1} - \vec{S}_i). \tag{13}$$

Thus, the average time evolution of the configuration obeys the *Aristotelian* or *overdamped* force–velocity relation:

$$\vec{\nabla}\mathcal{H} = \vec{F} = \mu\vec{vel}, \tag{14}$$

where $\mu$ is an *effective mobility*. The movements of individual boundary elements of a domain may be quite random, but the average velocities of large domains will be deterministic when the argument of the exponential in Eq.(10) is not too large.[5] When the argument is small enough, which is the case in most biological simulations, the deterministic velocity relationship is indeed linear and obeys Eq.(14), [70]. This result is the fundamental justification for using Metropolis-like dynamics in kinetic simulations. Changing the dynamics, *e.g.*, from Metropolis to Glauber, may change the results in complex and sometimes unpredictable ways [70].

Using Metropolis dynamics for kinetic simulations causes a number of problems. That Eq.(13) requires that the argument of the exponential in Eq.(10) be small, makes our original use of the Boltzmann factor in Eq.(9) questionable. However, no one has studied the effects on GGH modeling of switching to a different weighting factor in Eq.(9).

The exact relation between Monte-Carlo spin-copy attempts and continuous time are still the subject of debate and are a persistent source of criticism of kinetic applications of Metropolis-like algorithms in GGH simulations. In addition, because only the time-averaged movement obeys the deterministic kinetics, the time order of events occurring at different lattice sites is ambiguous over short times. Several more sophisticated approaches to dynamics are possible (see chapter II.4, section 3.1).

## 3. Kinetic Potts Simulations – From Metal Grains to Foams

### 3.1. From the Potts Model to Coarsening

The use of Metropolis methods to reveal the quasi-deterministic kinetics of configurations evolving under a Hamiltonian, led to a great expansion of the range of questions that Monte-Carlo methods could address. One new area of interest in the early 1980s was the kinetics of metallic grain growth. Most simple metals are composed of microcrystals, or *grains*, each of which has a particular crystalline lattice orientation. The atoms at the surfaces of these grains have a higher energy than those in the bulk because of their missing neighbors. We can characterize this

[5] Like a ferromagnet, the CPM has a critical temperature analogous to the Curie temperature (see section 6.1). Quasi-deterministic motion occurs only for temperatures well below this critical temperature.

excess energy as a *boundary energy*. Atoms in convex regions of a grain's surface have a higher energy than those in concave regions, in particular than those in the concave face of an adjoining grain, because they have more missing neighbors. Thus, an atom at a convex curved boundary can reduce its energy by "hopping" across the grain boundary to the concave side. The movement of atoms, which we can equivalently view as the movement of grain boundaries, lowers the net configuration energy, but requires thermal activation because an atom has a higher energy when it is in the space between grains than when it is part of one. Thus, while grains are stable at low temperatures, at high temperatures metallic microstructure changes through *annealing* or *coarsening*, with the net size of grains growing because of grain disappearance.

**3.1.1. The Exxon model of grain growth.** In the early 1980s, a group of researchers at Exxon Research, Michael P. Anderson, Gary S. Grest, Paradeep S. Sahni, and David J. Srolovitz, noticed that the Potts Hamiltonian is simply $J$ times the total boundary length of the configuration [45, 44, 46]. They drew an analogy between grain growth and the Potts model, where they took the lattice sites to correspond to atoms, the specific spin values to different crystalline orientations, and links between different spin domains to grain boundaries. They usually assumed that domains were initially connected and compact, with a different spin assigned to each grain to avoid grain coalescence.[6]

In grain growth *heterogeneous nucleation* does not occur, *i.e.* a spin of type $\sigma$ will not suddenly appear in the middle of a domain of spin $\sigma'$. Since the Metropolis algorithm allows heterogeneous nucleation, the Exxon group *modified* the *Metropolis algorithm* to prevent it by selecting the trial spin from the neighborhood of the target spin. We will call the lattice site of the trial spin $\vec{i}_{\text{source}}$ and its value $\sigma_{\text{source}}$ Though they did not recognize it at the time, the concept of a copy of lattice value with a source and target implied a copy *direction*, which proved crucial for later development of the GGH model. Forbidding heterogeneous nucleation means that evolution occurs only at domain boundaries. It also violates detailed balance, a further move away from statistical mechanics and towards purely kinetic modeling.

For low $T$, using the Potts Hamiltonian and the modified Metropolis dynamics, individual domains evolve in a manner that resembles the growth of metallic grains during annealing at high temperatures. The simulated evolution of the distributions of domain shapes, sizes and correlations agreed very well with experiments in metals [66].

**3.1.2. Coarsening in foams.** Glazier, working with the Exxon group, later showed that the simulated evolution also closely matched the experimental evolution of bubbles in 2D liquid soap froths, where gas diffuses across soap films depending on their curvatures [13, 15]. In this case, a link between two different spins represents

[6]Allowing multiple grains to have the same spin allows coalescence, which occurs in some metals. Since grain boundaries are simply links between lattice sites with different spins, when two grains with the same spin come into contact, they immediately fuse into one large grain.

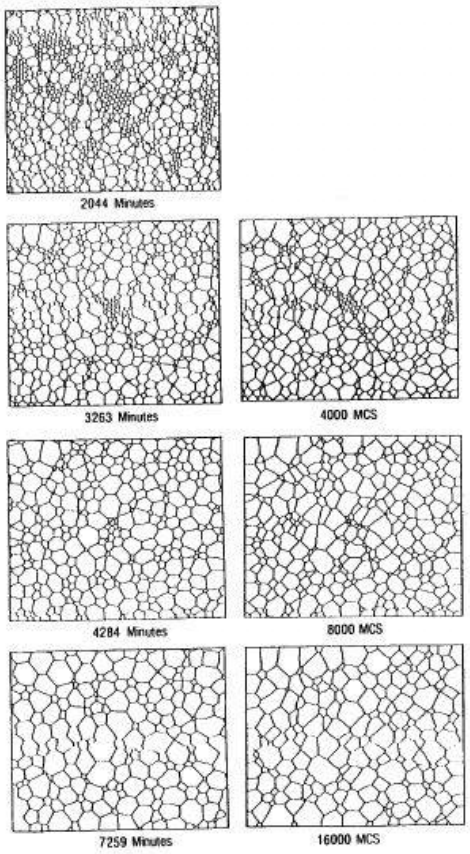


FIGURE 1. An evolving soap froth (left) and a large-$q$ Potts model simulation of grain growth (right) using the state of the soap froth at 2044 min as the initial condition. Adapted from [15].

a physical object, a unit of soap film, and the spins represent the gas inside the individual bubbles. The use of a mismatched link to represent a physical object – a soap film – was an important conceptual advance towards the GGH model. Glazier later extended these results to 3D [14]. Fig.1 shows the evolution of a soap froth and a Potts simulation using the configuration of the soap froth at 2044 min as its initial condition [15]. The use of Potts-derived models to study coarsening remains an active field of research [22, 30, 61, 60, 58]. For a review of the earlier history of this work, see [66].

**3.1.3. Lattice anisotropy.** The Exxon group's grain-growth simulations revealed a problem with the Potts approach. The energy of a unit of grain boundary is *anisotropic*; *i.e.*, it depends on the boundary's orientation with respect to the

lattice. Such lattice anisotropy can lead to alignment of grain boundaries along preferred axes, and even to boundary pinning at low temperatures. Holm *et al.*'s studies of these effects [23] led to the general adoption of longer interaction ranges for Potts simulations, *i.e.* when calculating the boundary energy, we consider $n^{th}$-nearest neighbors, where $n$ is an integer. Larger values of $n$ reduce lattice anisotropy effects, but increase computation time, compared to simulations with smaller values of $n$. Hexagonal lattices greatly reduce anisotropy compared to square lattices with the same neighbor range and are not difficult to implement computationally, but have not been much used in simulations. The optimum choice of lattice and the use of a distance-dependent $J$ factor to further reduce lattice anisotropy remain to be examined in a systematic fashion.

**3.1.4. Summary.** The Exxon simulations introduced many key ideas – the use of uniquely-labeled compact domains to identify different grains, the study of domain kinetics under the influence of boundary energy and fluctuations, the use of mismatched links to represent membranes, and the modification of the Metropolis algorithm to prevent heterogeneous nucleation. They also revealed the problem of lattice anisotropy, which still afflicts GGH simulations.

### 3.2. From Grains to Relaxed Foams – Constraints in an Extended Potts Model

One significant difference between foams and metallic grains is that the growth rate and relaxation rate of boundary shape of a metallic grain are the same, while in foams boundary relaxation is much faster than growth. The result is that grains can have irregular shapes, while foam boundary walls (soap films) are near-perfect minimal surfaces (circular arcs in 2D). In a brilliantly-presented and careful study, Weaire and Kermode extended the Potts model using constraints to simulate coarsening in 2D liquid foams [67, 68].

**3.2.1. Constraints.** The use of constraints to describe interactions comes from classical mechanics. *E.g.*, we can describe circular motion by imposing the constraint that a particle remains a constant distance from a specified point. We use the calculus of variations to derive equations of motion under a constraint, by minimizing an integral of a Hamiltonian (or Lagrangian) with an added physical *constraint condition*, which is the product of a *Lagrange multiplier*, $\lambda$ (the generalized force needed to maintain the constraint), with a function which is minimal when the constraint is satisfied.

In the context of Monte-Carlo dynamics, we can write a *constraint energy* in a general *elastic* form: $\lambda(value - target\ value)^2$. This constraint is zero if $value = target\ value$ and grows as *value* diverges from *target value*. We call the constraint *elastic*, because the exponent of 2 occurs in ideal springs and elastic solids (we could, in principle, use any positive even integer). Because the constraint energy decreases smoothly to a minimum when the constraint is satisfied, the modified Metropolis algorithm automatically drives any configuration towards one that satisfies the constraint. In the presence of multiple terms in a Hamiltonian, no constraint is usually satisfied exactly, because no configuration will satisfy

all constraints and minimize all energies simultaneously (see chapter II.2, section 5). While increasing the appropriate $\lambda$ can force the configuration to satisfy any constraint to any desired accuracy, increasing $\lambda/T$ reduces the acceptance rate, which slows the simulation timescale and makes it computationally inefficient. If $\lambda/T$ becomes too large, the simulation will *freeze* and only limited configuration evolution will occur. In the context of numerically solving differential equations, such constraints are appropriately called *stiff*. Since we can make *value* depend on the configuration in any way we want, and also make *target value* vary in any way we like in space or time, we can impose almost any behavior using constraints (although its expression may be cumbersome).

**3.2.2. The Weaire–Kermode model for soap froths.** Because Weaire and Kermode wanted domain growth to be slow compared to boundary relaxation and because they did not know that the domains in the large-$q$ Potts model already obeyed von Neumann's law [65], they added an elastic constraint on the volume of each domain and evolved the target volumes very slowly according to this law. They then used a Potts boundary-energy term in their Hamiltonian to impose an effective surface tension on their domains, causing boundaries to relax towards foam-like minimal-surface shapes [69]:

$$\mathcal{H} = J \sum_{(\vec{i},\vec{j})\,\text{neighbors}} (1 - \delta(\sigma(\vec{i}),\sigma(\vec{j}))) + \lambda \sum_{\sigma} (v(\sigma) - V_{\text{t}}(\sigma))^2, \tag{15}$$

where $\lambda$ is an inverse gas compressibility, $v(\sigma)$ is the number of lattice sites in the domain with spin $\sigma$, and $V_t(\sigma)$ is the target number of sites for that domain. One useful result from the constraint formalism is that $P \equiv -2\lambda(v(\sigma) - V_{\text{t}}(\sigma))$ is the *pressure* inside the domain. A domain with $v < V_{\text{t}}$ has a positive internal pressure, while a domain with $v > V_{\text{t}}$ has a negative pressure.

The shapes of the simulated domains in the Weaire–Kermode model were much more foam-like than those in Glazier's simulations. Unfortunately, this pioneering work was not followed up.

**3.2.3. Summary.** With Weaire and Kermode's extension of the Potts model to include a volume constraint [69], all that a model of biological cells still needed was a boundary energy that depended on domain type, an idea that goes back to the Heisenberg model of magnetism [72].

## 4. The Origin of the Cellular Potts Model

In this section we discuss the origin of the type-dependent boundary energies between cells used in the CPM and GGH model and write the full Hamiltonian for the CPM. The inspiration for the CPM came from experimental and theoretical work by the biologist Malcolm S. Steinberg at Princeton University on biological cell-sorting experiments and from later experiments on regeneration in aggregates of hydra cells (*Hydra vulgaris*) by the biophysicist Yasuji Sawada at Tohoku University, Sendai, Japan [48, 25, 42].

### 4.1. Cell Adhesion and Cell Sorting

Cell adhesion is fundamental to multicellular organisms, and to many unicellular organisms as well [10]. If cells could not stick to each other and to extracellular materials, building complex life would be impossible. Adhesion also provides a mechanism for controlling structures, as well as holding them together once they have formed.

In the late 1950s, Steinberg, while trying to understand how differences in gene expression between cells could translate into complex structures in embryos, noticed that during embryonic development, the behavior of aggregates of cells resembled the behavior of viscous fluids. For example, a random mixture of embryonic cells of two types, when formed into a 3D aggregate, reorganized into a compact ball with the more cohesive cell type surrounded by the less cohesive cell type in a phenomenon known as *cell sorting* [4, 3]. Differences in cohesion resulting from differences in the numbers and types of cell adhesion molecules on cell surfaces [11, 12, 9] could also explain the layered structure of the embryonic retina and the engulfment of a more cohesive tissue by a less cohesive tissue. Steinberg's *Differential Adhesion Hypothesis* (*DAH*) proposed that the final configuration of an initially arbitrary configuration of embryonic cells minimized their total free energy, so tissues really did behave like viscous fluids [54, 55, 56, 57].[7]

The many families of adhesion molecules (CAMs, cadherins, *etc.*) provided a mechanism for embryos to control the relative adhesivities of their various cell types to each other and to the noncellular ECM surrounding them, and thus to build complex structures. However, like the Ising model, the DAH was concerned only with equilibrium configurations, not kinetics.

### 4.2. The Cellular Potts Model

In 1991, Glazier joined the Sawada laboratory at Tohoku University in Sendai, Japan, which was famous for its studies on the regeneration of adult hydra from randomly mixed aggregates of their dissociated cells [48, 47, 49, 2, 53, 25, 42]. There, Glazier met Graner, who was studying the first phase of hydra regeneration, when endodermal cells sorted to the center of the aggregate and ectodermal cells to the surface [59]. Graner wanted to see if the DAH explained his results. Glazier realized that he could extend his foam simulations with the Exxon group to explore the kinetics and thermodynamics of biological cell sorting, *e.g.*, to determine whether the cell sorting that Steinberg and Armstrong had observed experimentally required active cell motility, which would imply that the energy landscape of the configuration space was *rough*, with many local minima, or could occur in the absence of fluctuations, which would imply that the energy landscape was *smooth*, with a single global minimum for the sorted state.

Glazier also realized that the domains could represent more than biological cells – in particular he introduced the concept of a domain as a *generalized cell*,

[7] In adult animal tissues and in plants, cells usually bind to each other tightly via specialized junctional structures and do not move relative to each other. Exceptions include wound healing, immune response and cancer.

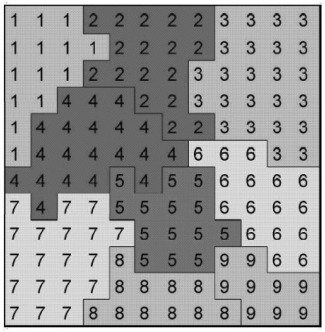


FIGURE 2. A typical configuration of the CPM or GGH model in 2D. The numerals indicate cell index values. The levels of gray indicate cell types. A cell is a collection of lattice sites with the same index value.

which could be a biological cell, a subelement of a cell, allowing compartmental cell models, or part of the extracellular medium, a fluid or a solid, depending on the domains' characteristics. This redefinition of *everything* in the simulation to be composed of generalized cells allows the same model to treat many different types of object, greatly simplifying model building.

Glazier and Graner's model discretized the continuous cell configuration onto a square lattice. A collection of lattice sites with the same index represented a generalized cell, as shown in Fig.2, with a unique index for each cell $\sigma(\vec{i}) \in [1, \ldots, N]$ defined at each lattice site $\vec{i}$, and a *cell type* $\tau(\sigma)$ for each cell. Links between different indices represented regions of contact between two cell membranes. From now on, we will drop the confusing term *spin* and refer to cell *indices*, since spin has no meaning in our biological context.

Since the cell volumes were constant and uniform in cell-sorting experiments, Glazier and Graner used an elastic volume constraint based on Weaire and Kermode's work on foams [69] to maintain the size of the biological cells. To represent variations in adhesion between cells of different types, they defined a Potts-like boundary energy which depended on the cell types at a link, $J(\tau(\sigma), \tau(\sigma'))$ (see Fig.2), so the boundary energy term in the Potts model (equation 4) became:

$$\mathcal{H}_{\text{boundary}} = \sum_{(\vec{i},\vec{j}) \text{ neighbors}} J(\tau(\sigma(\vec{i})), \tau(\sigma(\vec{j})))(1 - \delta(\sigma(\vec{i}), \sigma(\vec{j}))), \tag{16}$$

where the boundary energy coefficients are symmetric,

$$J(\tau, \tau') = J(\tau', \tau). \tag{17}$$

They assumed that the boundary energies were positive ($J > 0$), which proved to have unfortunate consequences (see section 6.2 below). The full Hamiltonian for

Glazier and Graner's CPM is:

$$\mathcal{H}_{\mathrm{CPM}} = \sum_{(\vec{i},\vec{j})\ \mathrm{neighbors}} J(\tau(\sigma(\vec{i})),\tau(\sigma(\vec{j})))(1-\delta(\sigma(\vec{i}),\sigma(\vec{j})))$$
$$+\sum_{\sigma}\lambda_{\mathrm{Vol}}(\tau)(v(\sigma)-V_{\mathrm{t}}(\tau(\sigma)))^2, \tag{18}$$

where, $v(\sigma)$ is the volume in lattice sites of cell $\sigma$, $V_{\mathrm{t}}$ its target volume, and $\lambda_{\mathrm{Vol}}(\tau)$ the strength of the volume constraint. In Glazier and Graner's original papers, the value of $V_{\mathrm{t}}$ was constant for all biological cells and the volume of the generalized cell representing the surrounding medium was unconstrained ($\lambda_{\mathrm{Vol}}(\mathrm{medium}) = 0$) [17, 16].

If we add a constant to all $J$s, and also add the same constant to the interaction energy between like indices (which is 0 in $\mathcal{H}_{\mathrm{contact}}$ in Eq.(18) and requires us to change the form of the equation), the evolution is unchanged. Since the kinetics in the modified Metropolis algorithm depends only on two things, the sign of $\Delta\mathcal{H}$ and the value of $\Delta\mathcal{H}/T$ (see Eq.(9)), if we multiply all the terms in the Hamiltonian by a positive constant and multiply the temperature as well, the evolution of configurations remains unchanged. Therefore, we have two degrees of freedom, one additive and one multiplicative, in setting the scale for the CPM parameters (see chapter II.2, section 4.1).

Since biological cells move actively (in the case of vertebrate cells usually by extending and retracting their membrane using their cytoskeletons), since these membrane fluctuations are very roughly analogous to thermal fluctuations (though they have a non-thermal origin) and since cells do not suddenly appear inside other cells, Glazier and Graner used the modified Metropolis algorithm of the Exxon Group for the dynamics of their model.

**4.2.1. Smoothing ("annealing").** The CPM runs with $T > 0$ and the usual values of of $\Delta\mathcal{H}/T$ are fairly small. Thus fluctuations are large, especially for more cohesive cells (those with lower $J$ values) and cell boundaries can become highly contorted. In this case, cells can become disconnected by spinning off small (usually single lattice-site) *blebs* (we take the name from the small membrane-encased blobs of cytoplasm which migrating cells sometimes leave behind). Neither blebs nor contorted boundaries are biologically realistic. Both can affect calculations of surface areas, neighbors and volumes. In Glazier and Graner's original papers, before they calculated statistics for a configuration, they eliminated disconnected blebs and smoothed cell boundaries by running their simulation with $T = 0$ for five, or more, MCS, using the normal Hamiltonian and modified Metropolis dynamics. Rather confusingly, they called this smoothing *annealing*, even though it is not the same as norm al annealing in metals. Later studies have generally not needed smoothing to reproduce biologically-observed behaviors.

## 5. Classical CPM Results

Because of Glazier and Graner's backgrounds in physics, their initial studies of cell sorting simulations resembled in many ways the Exxon group's statistical-mechanics studies of grain growth. They first validated the use of the CPM in a biological context by studying its phase transitions and the behaviors of simulated cells of a single type as a function of individual model parameters (*e.g.*, to establish the optimum range for $J/T$ and to check for excessive lattice-anisotropy effects). They then tried to simulate Steinberg and Armstrong's experiments on cell sorting, studying the behavior of mixtures of two types of cells, high-boundary-energy, low-adhesivity cells, and low-boundary-energy, high-adhesivity cells, surrounded by a single generalized cell representing fluid medium.

Their single most important result was to show that cell sorting is an activated process requiring membrane fluctuations [16]. In their CPM simulations at low temperatures, cells clustered but clusters could not coalesce. This observation was a good example of the way that simulations can clarify a complex experimental situation. Experiments had previously shown (and later experiments verified) that introducing drugs which blocked membrane fluctuations into the fluid medium containing the cell aggregates inhibited cell sorting [4, 36]. However, the drugs used interfered with the cells' cytoskeletons. Since the adhesion molecules, which determine cell-cell adhesivities, bind to the cytoskeleton and change their adhesivity when the cytoskeleton is disrupted, the experiments could not determine definitively whether the failure to observe sorting was due to lack of cell motility or to changes in cell-cell adhesivity. As in this case, biological experiments often lack clean control parameters. In their simulations, Glazier and Graner were able first to change cell motility while keeping adhesion constant and then to change cell adhesion while keeping cell motility constant. By comparing the results in these two cases, they were able to show that loss of cell motility indeed prevented sorting.

They then examined the various possible hierarchies of boundary energies ($J$s) to characterize the classes of typical patterns which they could obtain. The variety of outcomes, even in this very simple situation, showed the power of variations in the expression of cell adhesion molecules to control embryonic morphology (see a simulation MovII.1.1 form the accompanying DVD).

## 6. Peculiarities of the CPM

Glazier and Graner were trying to build a model so simple that they could understand the physics of all of its components. Thus the CPM has certain peculiarities, which, while not generally critical to biological simulations, may cause confusion and artifacts. If we are aware of these potential problems, we can usually take steps to make sure that they do not invalidate our results.

### 6.1. Temperature

We mentioned in section 5 that cell sorting (and indeed any interesting biological phenomenon we might want to investigate) requires cell motility both experimentally and in simulations. Thus we must pick a dynamics to go with our Hamiltonian. From a physical point of view, the modified Metropolis algorithm is the simplest choice.

Temperature can cause problems in a number of contexts in the CPM (see chapter II.2, section 6). The CPM has several phase transitions in temperature, three of which, in particular, are wholly non-biological and limit the range of temperatures which simulations can use. As a rough guide for picking appropriate values of $J$ to avoid ill effects, we want to accept a significant fraction of index-copy attempts but not so many that the lattice pattern melts. Thus we need $0.2 \leq \Delta\mathcal{H}/T \leq 2$. If the number of neighbors per lattice site is $n$, the typical fluctuation energy per index-copy is $Jn/2$, so we need to pick all of our $J$ values such that $0.2 < Jn/2T < 2$, which may not always be possible. If $J$ is too large relative to $T$ the boundaries of the cell will become rough and the cell will shed blebs. If $J$ is too small relative to $T$ the cell boundaries will become stiff and align with the lattice's preferred directions.

Only for small bacteria are actual thermal fluctuations important to motility. In all other cases, motility depends on molecular motors of varying kinds. The motivation for the use of the modified Metropolis dynamics was amoeboid motion of the mesenchymal cells in Steinberg and Armstrong's experiments, where fluctuations in a cell's cytoskeleton cause its membrane to *ruffle*, moving gently back and forth in a random manner. However, in most cases, cell motility results from different mechanisms [1], the geometries of which differ greatly from that of the typical membrane fluctuations in CPM cells.

Because active molecular motors drive all of these movements, the typical spectrum of membrane or cell movements need not follow the Boltzmann distribution of modified Metropolis dynamics. If the fluctuation spectrum of the movements matches the depth of local minima in a configuration-energy landscape, rearrangements may happen much faster than they would for thermal fluctuations, speeding the rate of configuration evolution. Worse, in almost every biological case, movements in a given direction tend to persist for fairly long times (up to a minute), because assembling and disassembling the molecular machinery responsible for cell movement takes time. Thus the assumption that motion is temporally uncorrelated, fails. We will discuss in chapter II.4, section 1.1 some ways to put these correlations back into GGH models. Sometimes these correlations have no significant effect. Unfortunately, when an energy landscape is rough, as it is for most biologically interesting problems, correlations and non-thermal fluctuation spectra can change not only time scales but time scaling [64]. Thus, in some cases, our assessment of the feasibility of a biological mechanism based on simulations may be incorrect.

Ironically, given these issues, the use of $T$ in GGH simulations has almost never been a significant limitation. Where it has, simple fixes like including an inertial constraint (see chapter II.4, section 1.1) seem to have solved the problem. Nevertheless, improving the realism of GGH kinetics is worthy of attention, experimentally (to characterize actual kinetics), computationally and theoretically (to understand the significance of different kinetic behaviors to configuration evolution and scaling).

### 6.2. Diffusion, Energy and Parameter Choices

Glazier and Graner's original model, following the physical reality in foams and metallic grains, assumed that boundary energies were positive, so the boundary energy term served both to minimize boundary areas and to determine the optimal arrangement of cells. A negative $J$ results in the cell boundaries breaking up to maximize their boundaries. When Glazier and collaborators began studying cell diffusion rates, they found that more cohesive cells (smaller $J > 0$) had more crumpled surfaces, larger membrane fluctuations, and diffused further than less cohesive cells, exactly the opposite of the expected result [42].[8] Since biological cells usually have adhesive interactions with each other and the ECM, the correct way to solve this problem is to use negative $J$ and constrain the surface area separately (see section 7.1.1). Equivalently, Hogeweg further modified the modified Metropolis dynamics by shifting the Boltzmann probability in Eq.(9) to negative $\Delta E_0$, which gives the same effect:

$$p(\sigma(\vec{i}_{\text{target}}) = \sigma_{\text{target}} \rightarrow \sigma(\vec{i}_{\text{target}}) = \begin{cases} 1 & \text{if } \Delta\mathcal{H} < \Delta E_0, \\ e^{-(\Delta\mathcal{H}-\Delta E_0)/T} & \text{if } \Delta\mathcal{H} \geq \Delta E_0. \end{cases} \tag{19}$$

We can equivalently view this modified dynamics as introducing an extra dissipation energy per index copy [31, 32]. Negative $J$s give correct diffusion hierarchies [42]. Since the configurations observed are independent of the sign of $J$ (only the diffusion constants are wrong), many researchers continue to use simpler $J > 0$ models, when they do not care about relative rates.

While relating GGH parameters to experimentally-meaningful material properties has proved difficult, the recent derivation of the continuous limit of the CPM may help to connect simulation and physical parameters [63].

### 6.3. Intrinsic Dissipation and Viscosity

To make CPM simulations mechanically realistic, we would like to be able to specify the resistance to motion that cells experience when moving through a fluid due to dissipation and viscosity. *Dissipation* is the loss of energy due to motion, *i.e.* resistance to all motion. *Viscosity* is dissipation which results from velocity gradients. The CPM is intrinsically dissipative, but not viscous. Consider a channel filled with CPM cells, which strongly adhere to the walls of the channel (small $J$). If we push the cells through the channel by applying a gradient, the cells will experience *plug flow*, *i.e.* all cells move with the same average velocity. The cells touching the walls do not move slower than those in the center of the channel, as

[8] In certain situations, strong binding between cells can lead to cytoskeletal changes which increase cell motility, in which case using positive energies may be more appropriate biologically.

we would expect in a viscous fluid. We can implement viscosity in the CPM (see chapter II.4, section 1.2.1) to produce the correct velocity profile. However, an object moving through a fluid with CPM viscosity experiences both viscous and intrinsic dissipation, while a real fluid has no intrinsic dissipation.

## 7. From the CPM to the GGH Model

The basic CPM models only the effects of differential adhesion, cell volume and fluctuations. The GGH model adds many of the other biological mechanisms we discussed in section 1 and also addresses some of the issues in section 6.

### 7.1. Simple Extensions to the Hamiltonian

**7.1.1. Surface area constraints and negative boundary energies.** Biological cells have a defined amount of cell membrane, which we can represent with a surface area constraint:

$$\mathcal{H}_{\text{surface}} = \sum_{\sigma} \lambda_{\text{S}}(\tau)(s(\sigma) - S_{\text{t}}(\tau(\sigma)))^2, \tag{20}$$

where $s(\sigma)$ is the surface area of cell $\sigma$ and $S_{\text{t}}$ is its target surface area in lattice sites. Changing the ratio:

$$R = \frac{3\sqrt{4\pi}S_{\text{t}}^{3/2}}{V_{\text{t}}}, \tag{21}$$

changes the rigidity of the cell. Like a slowly inflated balloon (which corresponds to decreasing $R$), for $R > 1$ the cell is floppy, while for $R = 1$ the cell is spherical and for $R < 1$ increasingly rigid. While Eq.(20) is the simplest form of surface area constraint, other forms are possible and may be preferable, *e.g.*:

$$\mathcal{H}'_{\text{surface}} = \sum_{\sigma} \lambda_{\text{S}}(\tau)\big(s(\sigma)v(\sigma)^{-2/3} - S_{\text{t}}V_{\text{t}}^{-2/3}\big)^2, \tag{22}$$

keeps the $R$ of a cell constant as it grows.

Constraining the cell surface area leaves us free to define cells' boundary energies $J$ to be either positive or negative, depending on their real biological values, eliminating the diffusion-hierarchy problem we noted in section 6.2.

### 7.2. Non-Hamiltonian Extensions

**7.2.1. Cell growth and proliferation.** The simplest way to simulate the growth of cells is to allow $V_{\text{t}}$ and $S_{\text{t}}$ to increase gradually with time from a given initial value, $V_{\text{t0}}$, to double that value, $2V_{\text{t0}}$ [7], at a rate proportional to the concentration of a nutrient or growth factor $C$ ([39], see also a simulation MovII.1.2 from the accompanying DVD):

$$\frac{dV_{\text{t}}}{dt} \propto C_{\text{growth factor}}. \tag{23}$$

For large $C$, a real cell's growth rate saturates, which we can include by replacing $C$ by a *Michaelis–Menten* or *Hill* form $\frac{C^{\alpha}}{\beta + C^{\alpha}}$, where $\alpha$ and $\beta$ are constants depending on cell type. Cells can also grow when they are stretched [43, 18].

**7.2.2. Cell division.** To model cell division (*mitosis*) when a cell $\sigma$ reaches a given doubling volume, we assign a new index $\sigma'$ to half of the existing cell's lattice sites, dividing the cell either along the cell's shortest axis [18, 19], or randomly [37, 39]. In both cases, the new cells have target volumes $V_{\mathrm{t}}/2$ [7]. The new target volumes ensure that the pressure inside the cells (chapter II.2, section 5) does not change during mitosis.

### 7.3. Fields, Forces and Diffusion

A key early GGH extension of the CPM was the inclusion of multiple, additional lattices to track the concentrations of molecules (or external driving potentials) that affect the cell behaviors. We refer to the lattice of cell indices as the *cell field* and the additional lattices as *external* or *auxiliary fields*. The CPM automatically handles contact forces between cells. However, we would like to describe other influences on cell movement as well, for instance, external physical forces, or indirect effects like chemotaxis. In the context of the GGH model, we implement any influence on cell movement either through a generalized potential energy added to the Hamiltonian or by directional biasing of index-copy acceptance probabilities. The latter has the form of a *generalized force* (chapter II.2, section 3).

The primary use of fields is to record the concentration of signaling chemicals or other biomolecules, which we will usually denote $C(\vec{i})$, that may diffuse and react (section 7.3.2) and influence cell behavior via chemotaxis (section 7.3.1) or in other ways. Usually simple fields are thought of as occupying the same space as the cell lattice (*i.e.* cells do not exclude fields), although we can use repulsive haptotaxis to keep cells and fields spatially distinct. Fields may also be attached to cells or subcells rather than to the lattice (see chapter II.4, section 1.2.2) in which case we denote the field $C(\sigma)$ and its value at a lattice site is:

$$C(\vec{i}) = C(\sigma(\vec{i}))v^{-1}(\sigma(\vec{i})), \tag{24}$$

*i.e.* the amount of chemical at a particular lattice site equals the amount in the cell divided by the cell volume.

In some simple cases, we can represent the field as an analytic function of position. *E.g.*, a graviational field in direction $\hat{n}$ produces a gravitational potential energy:

$$\mathcal{H}_{\mathrm{gravity}} = -\sum_{\vec{i}} \mu_{\mathrm{gravity}}(\tau(\sigma(\vec{i})))(\vec{i}\cdot\hat{n}), \tag{25}$$

where $\mu_{\mathrm{gravity}}(\tau(\sigma(\vec{i})))$ is the density of cell $\sigma$ [28].

Yi Jiang in her PhD thesis [27] applied shear forces directly to cells by including a term in the Hamiltonian of form:

$$H = \sum_{\vec{i}} f(\vec{i}, \sigma, t). \tag{26}$$

The force can depend on position, cell type and time.

**7.3.1. Chemotaxis and haptotaxis.** If cell adhesion is the most important biological mechanism permitting multicellularity (allowing cells to stick together to form larger groups), chemotaxis is the second most important (see chapter II.2, section 7.3). Adhesion by itself can only produce layers and blobs, while adhesion in conjunction with chemotaxis can produce a plausible facsimile of a multicellular organism like a slime mold [32]. Cells can respond to diffusible chemicals which may be present in the ECM (*chemotaxis*) as well as to chemicals bound to substrates (*haptotaxis*, which also includes cell movement in response to changes in substrate rigidity, texture or strain). Chemotaxis is crucial for long-range signaling during morphogenesis, allowing cells at one end of a tissue to control the motion of cells at the other end. Haptotaxis is crucial for shape stabilization. For example, pre-cartilage mesenchymal cells will travel to regions where the substrate has more non-diffusing fibronectin, where they will differentiate into cartilage and then bone.

The ability to simulate chemotaxis in the GGH model depends on cells responding in a simple fashion to external chemical gradients. The simplest prototype for such a response is if,

$$\vec{v} \propto \mu_{\text{cell}} \vec{\nabla} C, \tag{27}$$

where $C(\vec{x})$ is a chemical field and $\mu_{\text{cell}}$ is the cell's *chemotactic response* parameter. Then $C$ has the form of a *chemical potential* and $\mu_{\text{cell}} C$ has the form of a potential energy, so adding the term,

$$\mathcal{H}_{\text{chemotaxis}} = \mu_{\text{cell}} C(\vec{x}), \tag{28}$$

to the main Hamiltonian causes the cell to move up ($\mu < 0$) or down ($\mu > 0$) the chemical gradient.[9] Clearly this functional form is an oversimplification. Cells cannot respond to infinitely small gradients and cells do not go infinitely fast in large gradients. A sigmoidal response is more appropriate. Additionally, the value of $\mu$ is not static for a single cell. Cells *adapt* to external concentrations of chemicals, becoming less sensitive when chemical concentrations are high and more sensitive when they are low [52]. The timescale for adaptation varies greatly. In extreme cases cells respond only to abrupt temporal changes in chemical concentration rather than to spatial gradients.

Exactly how we translate the simple idea in Eq.(28) into an effective energy is somewhat complicated and depends on the idea of an index copy direction (see section 3.1.1), which corresponds physically to the direction of motion of a unit of cell membrane. The different implementations of chemotaxis/haptotaxis in the GGH model depend on whether we we consider the chemical field at the target lattice site only, at both the target and source lattice sites, or at the source lattice site only, and whether we use the chemotactic response of the source cell, target

[9] Most bacteria respond to chemical gradients in a totally different way, through *chemokinesis*. In this case, the bacterium moves (*runs*) in a roughly straight line for a period of time, then turns and randomizes its direction and moves off again in a straight line. If the external chemical concentration at the bacterium is increasing, the duration of the runs increases. If the concentration is decreasing, the duration of the runs decreases. The net result favors movement up the gradient and the net movement of the bacterium follows Eq.(28).

cell, or a combination. Depending on the particular biological situation, different choices may be appropriate. *E.g.*, when a cell forms a leading edge, it typically responds to chemical concentration changes at the leading edge only and not at the trailing edge, in which case we will want to consider the chemotactic response of the source cell only.

The simplest form of chemotaxis comes from [27],

$$\Delta\mathcal{H}_{\text{chemotaxis}} = (\mu(\sigma_{\text{target}}) - \mu(\sigma_{\text{source}}))C(\vec{i}_{\text{target}}). \tag{29}$$

This equation has the advantage that it has the potential energy form of Eq.(28). However, it only acts at boundaries between chemotacting differently cells. Thus, a big block of identically chemotacting cells will respond very weakly because they only sense the chemical field at their edges.

Savill and Hogeweg [50], in their models of *Dictyostelium discoideum* chemotaxis, used an energy change proportional to the difference between the local chemical concentrations at the destination and source sites:

$$\Delta\mathcal{H}_{\text{chemotaxis}} = \mu(\sigma_{\text{source}})(C(\vec{i}_{\text{source}}) - C(\vec{i}_{\text{target}})). \tag{30}$$

An advantage of this form is that a cell responds to a chemical field in the same way, regardless of what types of neighbors it has. Merks, in his model of vasculogenesis, modeled chemotaxis with contact inhibition, *i.e.* chemotaxis only at cell-medium interfaces, not at cell-cell interfaces [34]:

$$\Delta\mathcal{H}_{\text{chemotaxis}} = (\mu(\sigma_{\text{target}}) - \mu(\sigma_{\text{source}}))(C(\vec{i}_{\text{target}}) - C(\vec{i}_{\text{source}})). \tag{31}$$

CompuCell3D (see chapter II.4, section 5.1.1) [26] uses yet another form:

$$\Delta\mathcal{H}_{\text{chemotaxis}} = \mu(\sigma_{\text{source}})C(\vec{i}_{\text{target}}), \tag{32}$$

which can describe leading-edge-led cell movement. See also a simulation MovII.1.3 from the accompanying DVD. Finally, we know that for large $C$ or $\nabla C$, the cell's response saturates. We can include this effect using a Michaelis–Menten or Hill form:

$$\mathcal{H}_{\text{chemotaxis}} = \mu\frac{C^{\alpha}}{\beta + C^{\alpha}}. \tag{33}$$

Since all of these options may be appropriate in different biological circumstances, we propose to encapsulate all of them in a general term:

$$\Delta\mathcal{H}_{\text{chemotaxis}} = (a\mu(\sigma_{\text{source}}) + b\mu(\sigma_{\text{target}}))\frac{(cC(\vec{i}_{\text{source}}) - dC(\vec{i}_{\text{target}}))^{\alpha}}{\beta + (cC(\vec{i}_{\text{source}}) - dC(\vec{i}_{\text{target}}))^{\alpha}}, \tag{34}$$

where $a$, $b$, $c$, $d$, $\alpha$ and $\beta$ are constants. In particular, $\alpha$ is the Hill coefficient, which determines how steeply the chemotactic response rises at its threshold value $C{=}\beta$. To model haptotaxis [62, 73], we can use a chemotaxis form with a non-diffusing $C$ or make the surface energies $J'(\tau(\sigma(\vec{i})), \tau(\sigma(\vec{j})))$ depend on the concentration $C$. The simplest form is

$$J'(\tau(\sigma(\vec{i})), \tau(\sigma(\vec{j}))) = J(\tau(\sigma(\vec{i})), \tau(\sigma(\vec{j}))) - \beta\frac{C(\vec{i}) + C(\vec{j})}{2}, \tag{35}$$

where $\beta$ is a positive constant. The linear decrease of the values of $J'$, as the concentration of the chemical corresponding to cell adhesion molecules grows, leads to observed density-dependent patterns in mesenchymal condensation *in*

*vitro* where the average size of clusters is smaller at higher concentrations of these molecules, [73].

**7.3.2. Diffusion on external-field lattices.** Cells respond to diffusible signals from other cells or external sources. Typically, we implement diffusion using a separate solver which acts on the external fields, which we call a certain number of times per MCS. The simplest method, the *forward-Euler method*, evolves the diffusion equation by redistributing concentration between neighbor lattice sites from those with higher concentrations to those with lower concentrations. The proportion of concentration redistributed at each step relates to the diffusion constant for that substance. The Euler method is unstable when the ratio $D\Delta t/\Delta x^2$ is bigger than about $1/2^d$, where $d$ is the dimension of the space, but we can maintain stability by calling the diffusion solver multiple times per MCS and using a smaller $\Delta t$ each time.

An advantage of forward-Euler and other finite-difference schemes (for example, Crank–Nicholson) is that regions of the external field lattice corresponding to different cell types can have different secretion rates, decay rates and diffusion constants, including no diffusion and anisotropic diffusion. Since these properties correspond to individual cells (see section 7.4), which can move, we gain some of the benefits of advection–diffusion, at very little computational expense. For example, one iteration of a 2D diffusion equation with local decay rate $d(i,j)$ would be:

$$\begin{aligned} &C(i,j,t+\Delta t) = C(i,j,t) \\ &+D(i+1,j)C(i+1,j,t) + D(i,j+1)C(i,j+1,t) \\ &+D(i-1,j)C(i-1,j,t) + D(i,j-1)C(i,j-1,t) \\ &-4D(i,j)C(i,j,t) - d(i,j)C(i,j) + f(i,j)\Delta t, \end{aligned} \tag{36}$$

where $f(i,j)$ describes secretion, absorption and reaction of the chemical. This formula multiplies the concentration by the diffusion, secretion and decay rates site-by-site over the whole lattice prior to the iteration, which we sometimes call applying a *mask*. As the cell lattice evolves, the diffusion, secretion and decay rates update automatically.

### 7.4. Internal Cell States

As researchers have attempted more realistic biological simulations, they have devised methods to impart specific biological behaviors to individual cells. As a result, GGH simulations have focused more on the properties and interactions of generalized cells and less on the properties of individual lattice sites, though, of course, the actual movement of cells still occurs at the lattice-site level. This change in focus has inspired methods to describe and generate increasingly complex *internal cell states* and to describe generalized-cell interactions. We call this general class of approaches, *off-lattice extensions* of the GGH.

In Hogeweg's model of genetic evolution [18, 19, 21, 29], cells have simple models of a genome and intergenomic pathways that determine cell–cell adhesion, cell division and death. Between cell generations, the genetic code of each cell

evolves via gene mutations. The evolving regulatory pathways create cell colonies with unique morphogenetic tendencies, including many experimentally observed morphogenetic mechanisms and morphologies. Alternative methods for cell differentiation use preprogrammed type changes of the cells [51].

## 8. Outlook

The great advantages of the GGH model are its simplicity and extensibility, which have made it the most widely-used approach to cell-level modeling biology. GGH cells move according to effective-energy gradients $\vec{v} \propto \vec{\nabla}\mathcal{H}$, which means that $\vec{F} \propto \vec{v}$, as in biological experiments. As in experiments, the position and movement of membranes determine cell dynamics. Adding new biological mechanisms is as simple as adding new potential energies or constraints to the Hamiltonian. While the lattice discretization and modified Metropolis dynamics of the GGH model can cause certain artifacts, these rarely cause serious difficulties. Recent extensions of the GGH using subcells to model the behavior of fluids [8] and elastic media have addressed many of these issues (see chapter II.4, section 1). We discuss additional extensions to the GGH, which use generalized cells to provide many off-lattice enhancements to the GGH without abandoning the convenience of the GGH's underlying fixed lattice, in chapter II.4. As our understanding of the GGH model improves, we expect to be able to further improve both its accuracy and the range of biological problems it can address (see chapters II.2 and II.3) and to see it even more widely adopted.

This chapter has focused on the origin and development of the GGH model without discussing the computer-engineering aspects of its implementation. One of the most important developments in GGH modeling in the past few years has been the creation and release of open-source modeling packages like the *Tissue Simulation Toolkit* (*TST*) [33],[10] or *CompuCell3D* [26],[11] which provide standard platforms for model development (see the accompanying DVD for simulations: MovII.1.1, MovII,1,2 and MovII,1,3). The use of one of these standard packages allows users to reproduce published results and share new algorithms relatively painlessly, and opens the field of GGH modeling to a much broader audience.

**Acknowledgments**

We gratefully acknowledge support from the National Institutes of Health, National Institute of General Medical Sciences, grant 1R01 GM076692-01, an IBM Innovation Institute award, NASA Glenn Research Center, grant NAG 2-1619, the National Science Foundation, Division of Integrative Biology, grant IBN-0083653, and the Office of the Vice President for Research, the College of Arts and Sciences,

[10] http://sourceforge.net/projects/tst.

[11] http://dustbunny.physics.indiana.edu/∼mswat/wwwCompuCell/index.html,
https://simtk.org/home/compucell3d,
http://www.nd.edu/ lcls/compucell/linux.htm.

the Pervasive Technologies Laboratories, the AVIDD and ODIN computer clusters and the Biocomplexity Institute at Indiana University.

## References

[1] B. Alberts, A. Johnson, J. Lewis, M. Raff, K. Roberts, and P. Walter. *Molecular biology of the cell*. Garland, New York, 2002.

[2] H. Ando, Y. Sawada, H. Shimizu, and T. Sugiyama. Pattern formation in hydra tissue without developmental gradients. *Dev. Biol.*, 133:405, 1989.

[3] P. B. Armstrong and M. T. Armstrong. A role for fibronectin in cell sorting out. *J. Cell. Sci.*, 69:179, 1984.

[4] P. B. Armstrong and D. Parenti. Cell sorting in the presence of cytochalasin B. *J. Cell Biol.*, 55:542, 1972.

[5] J. Ashkin and E. Teller. Statistics of two-dimensional lattices with four components. *Phys. Rev.*, 64:178, 1943.

[6] S. G. Brush. History of the Lenz–Ising model. *Rev. Mod. Phys.*, 39:883, 1967.

[7] R. Chaturvedi, J. A. Izaguirre, C. Huang, T. Cickovski, P. Virtue, G. L. Thomas, G. Forgacs, M. S. Alber, S. A. Newman, and J. A. Glazier. Multi-model simulations of chicken limb morphogenesis. *Lect. Notes Comput. Sci.*, 2659:39, 2003.

[8] D. Dan, C. Mueller, K. Chen, and J. A. Glazier. Solving the advection–diffusion equations in biological contexts using the Cellular Potts model. *Phys. Rev. E*, 72:041909, 2005.

[9] G. Forgacs, R. A. Foty, Y. Shafrir, and M. S. Steinberg. Viscoelastic properties of living embryonic tissues: a quantitative study. *Biophys. J.*, 74:2227, 1998.

[10] G. Forgacs and S. A. Newman. *Biological physics of the developing embryo*. Cambridge Univ. Press, Cambridge, 2005.

[11] R. A. Foty, G. Forgacs, C. M. Pfleger, and M. S. Steinberg. Liquid properties of embryonic tissues: measurement of interfacial tensions. *Phys. Rev. Lett.*, 72:2298, 1994.

[12] R. A. Foty, C. M. Pfleger, G. Forgacs, and M. S. Steinberg. Surface tensions of embryonic tissues predict their mutual envelopment behavior. *Development*, 122:1611, 1996.

[13] J. A. Glazier. *Dynamics of cellular patterns*. PhD thesis, University of Chicago, 1989.

[14] J. A. Glazier. Grain growth in three dimensions depends on grain topology. *Phys. Rev. Lett.*, 70:2170, 1993.

[15] J. A. Glazier, M. P. Anderson, and G. S. Grest. Coarsening in the two-dimensional soap froth and the large-q Potts model: a detailed comparison. *Philos. Mag. B*, 62:615, 1990.

[16] J. A. Glazier and F. Graner. Simulation of the differential adhesion driven rearrangement of biological cells. *Phys. Rev. E*, 47:2128, 1993.

[17] F. Graner and J. A. Glazier. Simulation of biological cell sorting using a two-dimensional extended Potts model. *Phys. Rev. Lett.*, 69:2013, 1992.

[18] P. Hogeweg. Evolving mechanisms of morphogenesis: on the interplay between differential adhesion and cell differentiation. *J. Theor. Biol.*, 203:317, 2000.

[19] P. Hogeweg. Computing an organism: on the interface between informatic and dynamic processes. *Biosystems*, 64:97, 2002.

[20] P. Hogeweg. Computing an organism: on the interface between informatic and dynamic processes. In S. Kumar and P. J. Bentley, editors, *On growth, form and computers*, page 444. Elsevier, London, 2003.

[21] P. Hogeweg and N. Takeuchi. Multilevel selection in models of prebiotic evolution: compartments and spatial self-organization. *Orig. Life Evol. Biosph.*, 33:375, 2003.

[22] E. A. Holm and C. C. Battaile. The computer simulation of microstructural evolution. *JOM*, 53:20, 2001.

[23] E. A. Holm, J. A. Glazier, D. J. Srolovitz, and G. S. Grest. Effects of lattice anisotropy and temperature on domain growth in the two-dimensional Potts model. *Phys. Rev. A*, 43:2662, 1991.

[24] E. Ising. Beitrag zur Theorie des Ferromagnetismus. *Z. Physik.*, 31:253, 1925.

[25] T. Itayama and Y. Sawada. Development of electrical activity in regenerating aggregates of hydra cells. *J. Exp. Zool.*, 273:519, 1995.

[26] J. A. Izaguirre, R. Chaturvedi, C. Huang, T. Cickovski, J. Coffland, G. L. Thomas, G. Forgacs, M. S. Alber, H. G. E. Hentschel, S. A. Newman, and J. A. Glazier. Compucell, a multi-model framework for simulation of morphogenesis. *Bioinformatics*, 20:1129, 2004.

[27] Y. Jiang. *Cellular pattern formation*. PhD thesis, University of Notre Dame, 1998.

[28] Y. Jiang and J. A. Glazier. Extended large-q Potts model simulation of foam drainage. *Phil. Mag. Lett.*, 74:119, 1996.

[29] S. A. Kauffman. Metabolic stability and epigenesis in randomly constructed genetic nets. *J. Theor. Biol.*, 22:437, 1969.

[30] C. E. Krill and L. Q. Chen. Computer simulation of 3-D grain growth using a phase-field model. *Acta Mater.*, 50:3057, 2002.

[31] A. F. M. Marée and P. Hogeweg. How amoeboids self-organize into a fruiting body: multicellular coordination in *Dictyostelium discoideum*. *Proc. Natl. Acad. Sci. USA*, 98:3879, 2001.

[32] A. F. M. Marée and P. Hogeweg. Modelling *Dictyostelium discoideum* morphogenesis: the culmination. *Bull. Math. Biol.*, 64:327, 2002.

[33] R. M. H. Merks and J. A. Glazier. A cell-centered approach to developmental biology. *Physica A*, 352:113, 2005.

[34] R. M. H. Merks and J. A. Glazier. Dynamic mechanisms of blood vessel growth. *Nonlinearity*, 19:C1, 2006.

[35] N. Metropolis, A. W. Rosenbluth, M. N. Rosenbluth, A. H. Teller, and E. Teller. Equation of state calculations by fast computing machines. *J. Chem. Phys.*, 21:1087, 1953.

[36] J. C. Mombach, J. A. Glazier, R. C. Raphael, and M. Zajac. Quantitative comparison between differential adhesion models and cell sorting in the presence and absence of fluctuations. *Phys. Rev. Lett.*, 75:2244, 1995.

[37] J. C. M. Mombach, R. M. C. de Almeida, and J. R. Iglesias. Mitosis and growth in biological tissues. *Phys. Rev. E*, 48:598, 1993.

[38] L. Onsager. Crystal statistics. I. A two-dimensional model with an order–disorder transition. *Phys. Rev.*, 65:117, 1944.

[39] N. J. Popławski, M. Swat, J. S. Gens, and J. A. Glazier. Adhesion between cells, diffusion of growth factors, and elasticity of the AER produce the paddle shape of the chick limb. *Physica A*, 373:521, 2007.

[40] R. B. Potts. PhD thesis, University of Oxford, 1951.

[41] R. B. Potts. Some generalized order–disorder transformations. *Proc. Camb. Phil. Soc.*, 48:106, 1952.

[42] J. P. Rieu, A. Upadhyaya, J. A. Glazier, N. B. Ouchi, and Y. Sawada. Diffusion and deformations of single hydra cells in cellular aggregates. *Biophys. J.*, 79:1903, 2000.

[43] E. Ruoslahti. Stretching is good for a cell. *Science*, 276:1345, 1997.

[44] S. A. Safran, P. S. Sahni, and G. S. Grest. Kinetics of ordering in two dimensions. I. Model systems. *Phys. Rev. B*, 28:2693, 1983.

[45] P. S. Sahni, G. S. Grest, M. P. Anderson, and D. J. Srolovitz. Kinetics of the q-state Potts model in two dimensions. *Phys. Rev. Lett.*, 50:263, 1983.

[46] P. S. Sahni, D. J. Srolovitz, G. S. Grest, M. P. Anderson, and S. A. Safran. Kinetics of ordering in two dimensions. II. Quenched systems. *Phys. Rev. B*, 28:2705, 1983.

[47] M. Sato, H. R. Bode, and Y. Sawada. Patterning processes in aggregates of hydra cells visualized with the monoclonal antibody, Ts19. *Dev. Biol.*, 141:412, 1990.

[48] M. Sato and Y. Sawada. Regulation in the numbers of tentacles of aggregated hydra cells. *Dev. Biol.*, 133:119, 1989.

[49] M. Sato, H. Tashiro, A. Oikawa, and Y. Sawada. Patterning in hydra cell aggregates without the sorting of cells from different axial origins. *Dev. Biol.*, 151:111, 1992.

[50] N. J. Savill and P. Hogeweg. Modelling morphogenesis: from single cells to crawling slugs. *J. Theor. Biol.*, 184:229, 1997.

[51] N. J. Savill and J. A. Sherratt. Control of epidermal stem cell clusters by Notch-mediated lateral induction. *Dev. Biol.*, 258:141, 2003.

[52] G. Serini, D. Ambrosi, E. Giraudo, A. Gamba, L. Preziosi, and F. Bussolino. Modeling the early stages of vascular network assembly. *EMBO J.*, 22:1771, 2003.

[53] H. Shimizu, Y. Sawada, and T. Sugiyama. Minimum tissue size required for hydra regeneration. *Dev. Biol.*, 155:287, 1993.

[54] M. S. Steinberg. Reconstruction of tissues by dissociated cells. some morphogenetic movements and the sorting out of embryonic cells may have a common explanation. *Science*, 141:401, 1963.

[55] M. S. Steinberg. The problem of adhesive selectivity in cellular interactions. In M. Locke, editor, *Cellular membranes in development*, page 321. Academic, New York, 1964.

[56] M. S. Steinberg. Does differential adhesion govern self-assembly processes in histogenesis? equilibrium configurations and the emergence of a hierarchy among populations of embryonic cells. *J. Exp. Zool.*, 173:395, 1970.

[57] M. S. Steinberg and M. Takeichi. Experimental specification of cell sorting, tissue spreading and specific spatial patterning by quantitative differences in cadherin expression. *Proc. Natl. Acad. Sci. USA*, 91:206, 1994.

[58] A. Szolnoki and G. Szabo. Vertex dynamics during domain growth in three-state models. *Phys. Rev. E*, 70:027101, 2004.

[59] U. Technau and T. W. Holstein. Cell sorting during the regeneration of hydra from reaggregated cells. *Dev. Biol.*, 151:117, 1992.

[60] G. L. Thomas, R. M. C. de Almeida, and F. Graner. Coarsening of three-dimensional grains in crystals, or bubbles in dry foams, tends towards a universal, statistically scale-invariant regime. *Phys. Rev. E*, 74:021407, 2006.

[61] V. Tikare, E. A. Holm, D. Fan, and L. Q. Chen. Comparison of phase-field and Potts models for coarsening processes. *Acta Mater.*, 47:363, 1998.

[62] S. Turner and J. A. Sherratt. Intercellular adhesion and cancer invasion: a discrete simulation using the extended Potts model. *J. Theor. Biol.*, 216:85, 2002.

[63] S. Turner, J. A. Sherratt, K. J. Painter, and N. J. Savill. From a discrete to a continuous model of biological cell movement. *Phys. Rev. E*, 69:021910, 2004.

[64] A. Upadhyaya. *Thermodynamic and fluid properties of cells, tissues and membranes.* PhD thesis, University of Notre Dame, 2000.

[65] J. von Neumann. *Metal interfaces.* American Society for Metals, Cleveland, 1952.

[66] D. Weaire and J. A. Glazier. Modelling grain growth and soap froth coarsening: past, present and future. *Mater. Sci. Forum*, 94-96:27, 1992.

[67] D. Weaire and J. P. Kermode. Computer simulation of a two-dimensional soap froth. I. method and motivation. *Phil. Mag. B*, 48:245, 1983.

[68] D. Weaire and J. P. Kermode. Computer simulation of a two-dimensional soap froth. II. analysis of results. *Phil. Mag. B*, 50:379, 1984.

[69] J. Wejchert, D. Weaire, and J. P. Kermode. Monte Carlo simulation of the evolution of a two-dimensional soap froth. *Phil. Mag. B*, 53:15, 1986.

[70] S.-K. Wong. *A cursory study of thermodynamic and mechanical properties of Monte-Carlo simulations of the Ising model.* PhD thesis, University of Notre Dame, 2005.

[71] F. Y. Wu. The Potts model. *Rev. Mod. Phys.*, 54:235, 1982.

[72] K. Yosida. *Theory of magnetism.* Springer–Verlag, Heidelberg, 2006.

[73] W. Zeng, G. L. Thomas, and J. A. Glazier. A novel mechanism for biological cell clustering. *Physica A*, 341:482, 2004.

James A. Glazier
Biocomplexity Institute and Department of Physics, Indiana University
Swain Hall West 159, 727 East Third Street, Bloomington, Indiana 47405-7105, USA
e-mail: `glazier@indiana.edu`

Ariel Balter
Biocomplexity Institute and Department of Physics, Indiana University
Swain Hall West 117, 727 East Third Street, Bloomington, Indiana 47405-7105, USA
e-mail: `abalter@indiana.edu`

Nikodem J. Popławski
Biocomplexity Institute and Department of Physics, Indiana University
Swain Hall West 117, 727 East Third Street, Bloomington, Indiana 47405-7105, USA
e-mail: `nipoplaw@indiana.edu`